Infrared spectroscopic detection of the disilenyl (Si_2H_3) and d3-disilenyl (Si_2D_3) radicals in silane and d4-silane matrices

David Sillars [a], Chris J. Bennett [a], Yoshihiro Osamura [b], Ralf I. Kaiser [a,*]

[a] *Department of Chemistry, University of Hawai'i at Manoa, 2545 The Mall, Honolulu, HI 96822, USA*
[b] *Department of Chemistry, Rikkyo University, 3-34-1 Nishi-ikebukuro, Tokyo 171-8501, Japan*

Received 30 December 2003; in final form 26 May 2004
Available online 20 June 2004

Abstract

The disilenyl, $H_2SiSiH(X^2A)$, and the d3-isotopomer were detected for the first time via infrared spectroscopy in low temperature silane matrices upon an irradiation of the sample matrices with energetic electrons. The v_5 fundamental was observed at 651 and 493 cm^{-1}, respectively. In the d4-silane matrix, the v_4 at 683 cm^{-1} was noticed, too. Our investigations suggest that this radical is formed via radiolysis of silylsilylene, $H_3SiSiH(X^1A')$, and disilene, $H_2SiSiH_2(X^1A_g)$. The new absorption of the $H_2SiSiH(X^2A)$ radical may be employed in future spectroscopic monitoring of chemical vapor deposition processes and in astronomical searches of silicon-bearing molecules toward the carbon star IRC + 10216.
© 2004 Elsevier B.V. All rights reserved.

1. Introduction

In recent years, the structures, energetics, and spectroscopic properties of small hydrogenated silicon clusters of the generic formula Si_xH_y ($x = 1$, 2; $y = 1$–6) attracted considerable attention [1–6]. Due to their technological applications such as silane chemical vapor deposition and semiconductor processing, a detailed understanding of the structures and energetics of these clusters is also of fundamental interest in solid state chemistry and physics [7]. Here, plasma etching processes, reactive plasmas, and chemical vapor deposition techniques are of wide technological interest to produce silicon-bearing nano-particles and also amorphous silicon films (a-Si:H) [8]. The latter have fundamental applications in material sciences, particularly in the development of solar cells, electro-photographic drums, and arrays for liquid crystal displays. In chemical vapor deposition processes, silane (SiH_4) or disilane (Si_2H_6) are decomposed by hot filaments or electrons generated within plasmas [9]. During these procedures, silicon-bearing species such as SiH_y ($y = 1$–3) and clusters like

Si_2H_y ($y = 1$–5) have been identified in the gas phase as major growth species to produce amorphous, often porous silicon films [10–12].

Identifying the controlling and growth-limiting reactions for the production of amorphous silicon films requires a rigorous knowledge of the time-dependent concentrations of silicon-bearing species in actual chemical vapor deposition processes. The in situ characterization of gaseous species in CVD processes is predominantly carried out via time resolved threshold ionization mass spectrometry such as of the disilyl radial, $Si_2H_5(X^2A')$ [9,13–15]. Despite the importance of the Si_2H_y ($y = 1$–5) species in chemical vapor deposition processes, no time resolved spectroscopic probes have been established. Here, a detailed knowledge of the infrared absorption features might help to follow the chemical evolution of silicon CVD process not only via mass spectrometry, but also through time resolved infrared spectroscopy. So far, the most intense vibrational levels of disilane, $Si_2H_6(X^1A_{1g})$ [2158 cm^{-1}, 841–835 cm^{-1}] [16], of the disilyl radical, $Si_2H_5(X^2A')$ [843 cm^{-1}] [17], of two Si_2H_4 isomers disilene (H_2SiSiH_2, X^1A_g) [904, 2180, 2201 cm^{-1}] [18] and silylsilylene (HSiSiH_3, X^1A') [707, 861–857, 1963, 2112, 2154–2145, 2167 cm^{-1}] [16,18], and of the dibridged Si_2H_2 species [1093–1100

cm^{-1}] [16] have been determined experimentally in low temperature matrices. It is fairly surprising that no infrared spectroscopic, but only a Fourier transform microwave investigation on any Si_2H_3 isomers has been carried out to date [19].

Our investigations are also valuable to contribution to a detection of hitherto unidentified silicon-bearing molecules in the circumstellar envelopes of the carbon star IRC + 10216. So far, seven silicon containing species, i.e., silicon carbide (SiC), silicon nitride (SiN), silicon cyanide (SiCN), and tetracarbonsilicate (CCCCSi) together with two cyclic molecules (SiC_2, SiC_3) have been detected in this stellar outflow [20,21]. Here, the silane molecule – a potential precursor to complex organo-silicon molecules – has also been detected in the outflow of IRC + 10216 via infrared telescopes [22].

In this Letter, we present a combined experimental and theoretical study on the infrared spectroscopic detection of the Si_2H_3 radical and its deuterated counterpart in low temperature silane and d4-silane matrices. We have demonstrated earlier that in low temperature methane matrices, energetic electrons induce primarily a carbon–hydrogen bond cleavage to form a methyl radical and atomic hydrogen ($CH_3(X^2A_2'') + H(^2S_{1/2})$). Neighboring methyl radicals were found to recombine to an ethane molecule, $C_2H_6(X^1A_{1g})$. A consecutive irradiation of the sample with higher electron currents lead to a successive loss of hydrogen atoms via the reaction sequence $C_2H_6(X^1A_{1g}) \rightarrow C_2H_5(X^2A') \rightarrow C_2H_4(X^1A_g) \rightarrow C_2H_3(X^2A') \rightarrow C_2H_2(X^1\Sigma_g^+)$. Recently, a similar approach was utilized to form the disilyl radical, $Si_2H_5(X^2A')$, in silane matrices. In this Letter, we expand this protocol and synthesize the Si_2H_3 radical via Si_2H_4 isomers in SiH_4 and SiD_4 ices, $Si_2H_6(X^1A_{1g}) \rightarrow Si_2H_5(X^2A') \rightarrow Si_2H_4$ isomers $\rightarrow Si_2H_3$ isomers. These studies provide the position of the most intense, hitherto elusive infrared absorption frequencies of these species. Complete descriptions of the Si_2H_3 and Si_2H_4 potential energy surfaces are given in a forthcoming publication.

2. Experimental

The laboratory experiments were conducted in an ultrahigh vacuum (UHV) chamber. Briefly, the vessel consists of a cylindrical stainless steel chamber which can be pumped down to 2×10^{-10} Torr by a magnetically suspended turbopump backed by an oil-free scroll pump. A two stage closed cycle helium refrigerator is interfaced to the machine carrying a polished silver crystal. Cooled to 10.4 ± 0.2 K, the latter serves as a substrate for the ice condensate. The silane and d4-silane ice were prepared at 10 K by condensing silane (99.99%) and d4-silane (99.99%) at pressures of 5–6×10^{-8} Torr for 30 min onto the silver target. A
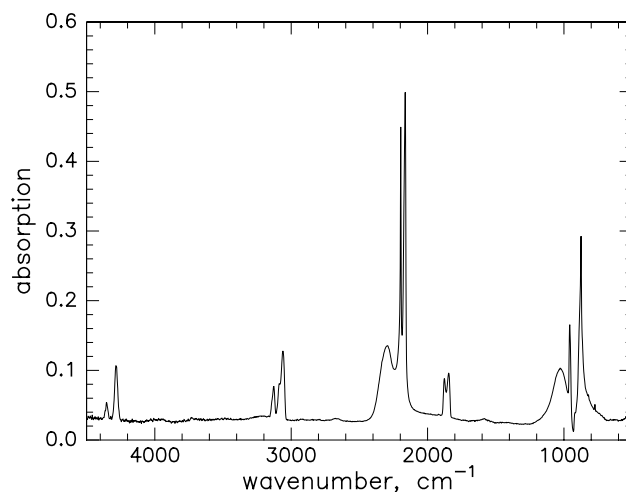
Fig. 1. Infrared spectrum of the silane frost at 10 K. The assignments of the peaks are compiled in Table 1.

comparison of our data (Fig. 1 and Table 1) with the literature data suggests that the frozen high temperature modifications of $SiH_4(I)$ and $SiD_4(I)$ dominate the constitution of the sample. However, the presence of a v_2 peak at 957 cm^{-1} which is infrared inactive in crystalline $SiH_4(I)$ suggests that the sample is partially disordered, possibly amorphous. We would like to stress that $SiH_4(II)$ can be excluded because we do not observe any fine structure in v_3 (2163 cm^{-1}) and v_4 (876 cm^{-1}). To determine the ice thickness, the infrared absorption features at 2163 and 876 cm^{-1} were integrated; the ice thickness was calculated then via the Lambert–Beer relationship [23]. Considering the integrated absorption coefficients of these fundamentals, i.e., 2.5×10^{-17} and 2.0×10^{-17} cm, and a density of the silane ice of

Table 1
Infrared absorptions of the silane frosts (sh: shoulder); α, β, and γ denote lattice modes of the silane sample

Frequency (cm^{-1})	Assignment
4354	$2 v_3$
4283	$v_1 + v_3$
3142 (sh)	$v_3 + v_4 + \beta$
3128	$v_2 + v_3$
3087	$v_3 + v_4 + \alpha$
3060	$v_3 + v_4$
2300	$v_3 + \gamma$
2250	$v_3 + \beta$
2195	$v_3 + \alpha$
2163	v_3
1876	$v_2 + v_4 + \alpha$
1844	$v_2 + v_4$
1050	$v_2 + \beta/v_4 + \gamma$
957	v_2
948	$v_4 + \beta$
918	$v_4 + \alpha$
876	v_4

0.77 ± 0.03 g cm^{-3} [24], an optical thickness of 0.2 μm silane was derived.

These ices were irradiated at 10 K with 5 keV electrons generated in an electron gun at beam currents of 1000 nA by wobbling the electron beam over the target area of 3.0 ± 0.4 cm^2. Accounting for irradiation times of between of 120 min and the extraction efficiency of 78.8% of the electrons, this exposes the targets to 4.5×10^{16} electrons. To guarantee an identification of the reaction products in the ices a Fourier transform infrared spectrometer was utilized. The Nicolet 510 DX FTIR machine (5000–500 cm^{-1}) operated in an absorption–reflection–absorption mode (reflection angle $\alpha = 75°$) (resolution 0.5–2 cm^{-1}). The infrared beam was coupled via a mirror flipper outside the spectrometer, passed through a differentially pumped potassium bromide (KBr) window, was attenuated in the ice sample prior and after reflection at a polished silver waver, and exited the main chamber through a second differentially pumped KBr window before being monitored via a liquid nitrogen cooled detector.

3. Theoretical approach

The molecular structures of various isomers for the Si_2H_2, Si_2H_3, and Si_2H_4 species were optimized in terms of ab initio density functional B3LYP methods [25,26] with the 6-311G(d,p) basis set [27]. Most of the structures of Si_2H_3 and Si_2H_4 have been studied previously [28,19], but we have calculated the vibrational frequencies and infrared intensities for these Si_2H_n species and their deuterated Si_2D_n counterparts to identify the newly formed silicon-bearing species unambiguously. The coupled cluster CCSD(T) calculations [29,30] with the aug-cc-pVTZ basis set [31] were also performed at the optimized structures obtained with the B3LYP method in order to compare the relative energies of various isomers. All computations were carried out using the Gaussian 98 program package [32]. The relative energies stated in the text are the values obtained with the CCSD(T) method corrected with the zero-point vibrational energies obtained with the B3LYP method (Tables 2 and 3).

4. Results

Our spectroscopic studies suggest that the response of the silane system upon the electron bombardment is governed by an initial formation of the silyl radical, $SiH_3(X^2A_1)$, plus atomic hydrogen. Here, absorption features of the silyl and d3-silyl radicals are observable immediately at 722 cm^{-1} (v_2; SiH_3) as well as 540 cm^{-1} (v_2; SiD_3) and 669 cm^{-1} (v_4; SiD_3) [17]. The v_2 peak agrees well with previous matrix studies [33–35]. Strong

absorptions at 820 cm^{-1} (v_6; $Si_2H_6(X^1A_{1g})$) and 935 cm^{-1} (v_8; $Si_2H_6(X^1A_{1g})$) as well as at 606 cm^{-1} (v_6; $Si_2D_6(X^1A_{1g})$) and 1541 cm^{-1} (v_5; $Si_2D_6(X^1A_{1g})$) were observable, too. Mechanistical studies suggested that the disilane molecule was formed via recombination of two *neighboring* silyl radicals (reactions (1) and (2)) [17]:

$$SiH_4(X^1A_1) \rightarrow SiH_3(X^2A_1) + H(^2S_{1/2}) \qquad (1)$$

$$SiH_3(X^2A_1) + SiH_3(X^2A_1) \rightarrow Si_2H_6(X^1A_{1g}). \qquad (2)$$
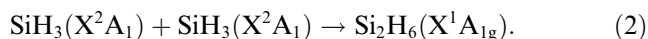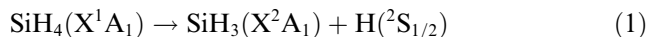
We would like to stress that the assignment of all peaks was double checked in perdeuterated silane (SiD_4) matrices. Here, we detected two fundamentals of the d3-silyl radical, $SiD_3(X^2A_1)$, at 669 cm^{-1} (v_4; shoulder) and 540 cm^{-1} (v_2; Fig. 3); this assignment corresponds very well with previously assigned peak positions at 668 cm^{-1} and about 546 cm^{-1} in noble gas matrices. Likewise, the d6-disilane molecule was observed in our experiments through its absorptions at 606 cm^{-1} (v_6; Fig. 2) and 1541 cm^{-1} (v_5). Summarized, at low irradiation currents of 10 nA, solely absorptions of the silyl radical, $SiH_3(X^2A_1)$, and of the disilane molecule, $Si_2H_6(X^1A_{1g})$, together with their deuterated counterparts can be observed unambiguously in the silane matrix (Table 4). As the irradiation time increases, previous studies shows also the formation of the disilyl radical, $Si_2H_5(X^2A')$, via reaction (3). Here, absorptions could be detected at 843 cm^{-1} (v_6; $Si_2H_5(X^2A')$) and 621 cm^{-1} (v_6; $Si_2D_5(X^2A')$)

$$Si_2H_6(X^1A_{1g}) \rightarrow Si_2H_5(X^2A') + H(^2S_{1/2}) \qquad (3)$$

Having identified the disilyl radical as a radiolysis product of the disilane molecule, we investigate now how the system responds on significantly enhanced exposure to electrons. As the irradiation time increases, new absorptions appear at 867 cm^{-1} (silane matrix; Fig. 2) and 635 cm^{-1} (d4-silane matrix, Fig. 2). A shoulder is also observable at 528 cm^{-1} in the d4-silane matrix. Since our goal is to observe the reaction sequence (4) in a similar manner as carried out previously in methane samples (reaction sequence (5)), we compare the observed absorptions with those computed for the three energetically most stable Si_2H_4 isomers (Table 2):

$$Si_2H_6(X^1A_{1g}) \rightarrow Si_2H_5(X_2A') \rightarrow Si_2H_4 \rightarrow Si_2H_3 \qquad (4)$$

$$C_2H_6(X^1A_{1g}) \rightarrow C_2H_5(X^2A') \rightarrow C_2H_4(X^1A_g)$$
$$\rightarrow C_2H_3(X^2A') \rightarrow C_2H_2(X^1\Sigma_g^+). \qquad (5)$$
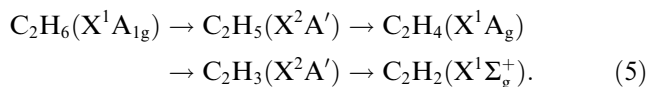
Indeed, the 867 and 635 cm^{-1} modes can be clearly identified as the most intense v_5 fundamental (umbrella mode of the SiH_3/SiD_3 group) of the $H_3SiSiH(X^1A')$ isomer and its isotopomer. The 528 cm^{-1} peak correlates nicely with the Si–D-bending mode of the D_3Si-$SiD(X^1A')$ species (Table 2). Scaling the computed frequencies with a factor of 0.99 yields an excellent

Table 2
Unscaled vibrational frequencies (cm^{-1}) and their infrared intensities (km mol^{-1}) of the three lowest energy Si_2H_4 and Si_2D_4 isomers calculated with B3LYP/6-311G(d,p) method

Symmetry	Frequency	Intensity	Frequency	Intensity	Characterization
C_{2h}	**1a** $H_2SiSiH_2(X^1A_g)$		D_2SiSiD_2		
v_1 (a_g)	2229	0	1596	0	Sym. SiH str.
v_2 (a_g)	956	0	713	0	Sym. SiH_2 bend
v_3 (a_g)	562	0	614	0	Si–Si str.
v_4 (a_g)	324	0	254	0	Rock
v_5 (a_u)	2258	148	1634	79	Asym. SiH str.
v_6 (a_u)	525	0	371	0	Torsion
v_7 (a_u)	348	23	249	12	Deform
v_8 (b_g)	2246	0	1625	0	Asym. SiH str.
v_9 (b_g)	616	0	469	0	Deform
v_{10} (b_u)	2225	110	1590	61	Sym. SiH str.
v_{11} (b_u)	920	183	665	95	Sym. SiH_2 bend
v_{12} (b_u)	447	32	327	17	Rock
C_s	**1b** $H_3SiSiH(X^1A')$		D_3SiSiD		
v_1 (a')	2214	128	1597	75	SiH str.
v_2 (a')	2179	76	1553	40	Sym. SiH str.
v_3 (a')	2037	206	1465	106	SiH str.
v_4 (a')	933	71	671	60	SiH_3 deform
v_5 (a')	868	222	641	78	SiH_3 umbrella
v_6 (a')	716	62	533	42	SiH bend
v_7 (a')	426	24	377	16	Rock
v_8 (a')	368	8	288	9	Si–Si str.
v_9 (a'')	2188	109	1580	63	Asym. SiH str.
v_{10} (a'')	957	38	686	21	SiH_3 deform
v_{11} (a'')	386	29	280	15	Deform
v_{12} (a'')	51	10	37	5	Torsion
C_1	**1c** $H_2SiHSiH(X^1A)$		$D_2SiDSiD$		
v_1 (a)	2220	127	1604	72	Asym. SiH_2 str.
v_2 (a)	2196	148	1573	82	Sym. SiH_2 str.
v_3 (a)	2041	178	1468	90	SiH str.
v_4 (a)	1627	117	1168	59	Bridge H str.
v_5 (a)	1009	356	732	185	Bridge H shift
v_6 (a)	962	38	688	7	SiH_2 scissor
v_7 (a)	858	88	615	43	Bridge H deform
v_8 (a)	703	37	538	38	Rock
v_9 (a)	636	7	453	2	Twist
v_{10} (a)	477	27	442	11	Si–Si str.
v_{11} (a)	448	3	344	7	Deform
v_{12} (a)	396	6	285	4	Rock

agreement with our experimental observations. The computed integral absorption coefficients also suggest that the v_5 band of $H_3SiSiH(X^1A')$ is the strongest one. The remaining absorptions, e.g., the Si–H and Si–D stretching modes, are either obscured by the silane matrices or are too weak to be detectable. It is important to note that at 10 K, we were not able to detect any absorption of the thermodynamically more stable $H_2SiSiH_2(X^1A_g)$ isomer. Our calculations suggest that the $H_2SiSiH_2(X^1A_g)$ structure is favorable by about 25 kJ mol^{-1} (27 kJ mol^{-1} is the value with CCSD(T) method) compared to $H_3SiSiH(X^1A')$; this agrees well with a recent study which obtained a value of 27.3

kJ mol^{-1} [19]. Here, the most intense v_{11} mode of $H_2SiSiH_2(X^1A_g)$ lies within the v_4 and $v_4 + \alpha$ absorptions of the silane matrix (Table 1). Also, we would like to stress that the thermodynamically even less stable, hydrogen bridged $H_2SiHSiH(X^1A)$ isomer is not detectable either (we computed that the $H_3SiSiH(X^1A')$ structure is favored by about 3 kJ mol^{-1} compared to the $H_2SiHSiH(X^1A)$ isomer; again, this order of magnitude compares well with Sari's et al. data of 3 kJ mol^{-1}). If it existed, the v_3 mode should be observable in our experiment. Therefore, we can conclude that $H_2SiHSiH(X^1A)$ is not formed. This correlates nicely with the failed detection of the hydrogen-bridged

Table 3
Unscaled vibrational frequencies (cm^{-1}) and their infrared intensities (km mol^{-1}) of the three lowest energy Si_2H_3 and Si_2D_3 isomers calculated with B3LYP/6-311G(d,p) method

Symmetry	Frequency	Intensity	Frequency	Intensity	Characterization
C_1	**2a** $H_2SiSiH(X^2A)$		D_2SiSiD		
v_1 (a)	2210	121	1596	68	Asym. Si–H str.
v_2 (a)	2180	109	1562	57	Sym. Si–H str.
v_3 (a)	2041	182	1468	92	Si–H str.
v_4 (a)	965	93	702	42	SiH_2 scissor
v_5 (a)	683	24	511	18	Rock
v_6 (a)	448	6	422	7	Deform
v_7 (a)	402	9	298	4	Out-of-plane
v_8 (a)	385	13	279	7	Deform
v_9 (a)	192	7	142	4	Torsion
C_s	**2b** $H_3SiSi(X^2A'')$		D_3SiSi		
v_1 (a')	2188	115	1573	68	Asym. Si–H str.
v_2 (a')	2155	74	1540	39	Sym. Si–H str.
v_3 (a')	953	68	684	44	Si–H str.
v_4 (a')	866	254	641	112	SiH_2 scissor
v_5 (a')	407	18	382	19	SiH_3 deform
v_6 (a')	295	27	226	17	Sym. bend
v_7 (a'')	2191	115	1583	65	Asym. bend
v_8 (a'')	911	44	654	23	Deform
v_9 (a'')	386	12	286	6	Rock
C_s	**2c** $H_2SiHSi(X^2A'')$		D_2SiDSi		
v_1 (a')	2179	157	1559	88	Sym. Si–H str.
v_2 (a')	1662	109	1193	54	Bridge H str.
v_3 (a')	972	365	711	176	Scissor
v_4 (a')	930	57	662	23	H bend
v_5 (a')	470	24	459	30	Si–Si str.
v_6 (a')	425	22	319	13	SiH_2 rock
v_7 (a'')	2189	125	1583	71	Asym. Si–H str.
v_8 (a'')	726	24	519	13	Twist
v_9 (a'')	407	7	302	4	Deform

$HSiHSiH_3$ isomer which cannot be formed by a Si–H bond rupture from disilane.

As the irradiation time increases even further, we detected additional bands at 651 cm^{-1} (Fig. 3; silane target) as well as 493 and 683 cm^{-1} (Fig. 3; d4-silane). These absorptions cannot be attributed to any Si_2H_x/Si_2D_x ($x = 4–6$) isomer. Instead, we compared these data with the energetically most stable Si_2H_3/Si_2D_3 structures – assuming that the newly observed bands originate from an electron-induced decomposition of the Si_2H_4/Si_2D_4 isomers. Here, we can verify the existence

of the $H_2SiSiH(X^2A)$ isomer together with its perdeuterated isotopomers via the v_5 (rocking) and v_4 (SiH_2 scissor; shoulder) fundamentals. A scaling factor of about 0.97 converts the computed frequencies to the experimentally observed ones. In case of $H_2SiSiH(X^2A)$, the more intense $v_1–v_4$ modes overlap with those of the silane molecule; likewise, the $v_1–v_3$ modes of $D_2SiSiD(X^2A)$ cannot be observed (Table 4). Therefore, not only the microwave transitions [19], but also the infrared absorption can be utilized in future spectroscopic searches of the $H_2SiSiH(X^2A)$ radical. Compared to the

Table 4
Compilation of newly observed Si_2H_4, Si_2H_3, and Si_2H_2 species together with their deuterated counterparts in low temperature silane matrices

Species	Frequency (cm^{-1})	Fundamental	Frequency (cm^{-1})	Species
H_3SiSiH	867	v_5	635	D_3SiSiD
H_3SiSiH	–	v_6	528 (sh)	D_3SiSiD
H_2SiSiH_2	*898*	*v_{11}*	*658*	*D_2SiSiD_2*
H_2SiSiH	651; 641(sh)	v_5	493	D_2SiSiD
		v_4	683(sh)	

Absorptions in italics were observed after the sublimation of the silane matrices (sh: shoulder).
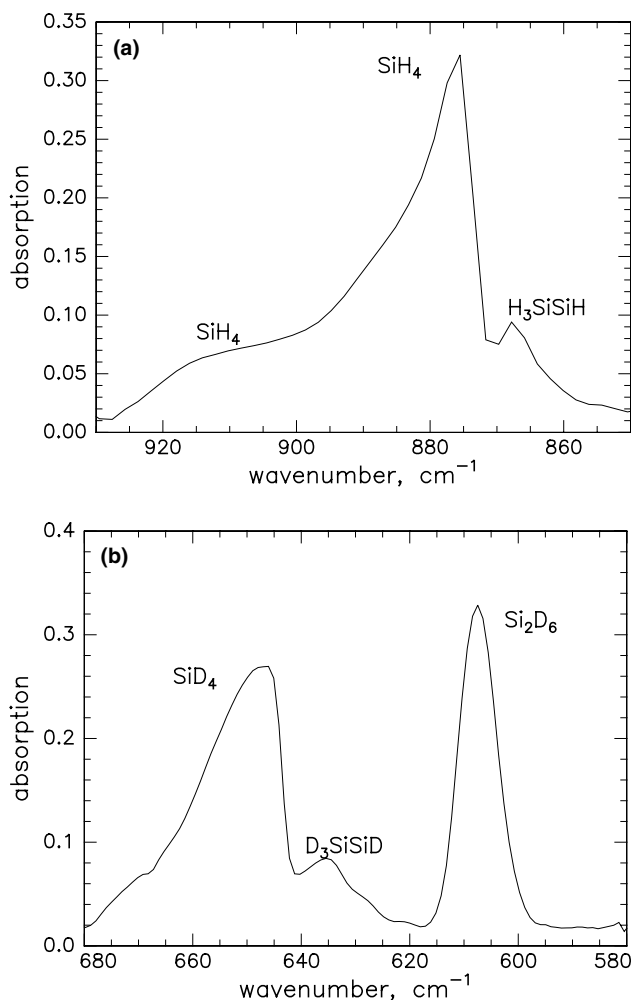
Fig. 2. New absorption features of the silylsilylene (HSiSiH$_3$, X^{1}A′) isomer at 867 cm^{-1} (a) and of the d4-silylsilylene (DSiSiD$_3$, X^{1}A′) isomer at 635 cm^{-1} (b) in the silane and d4-silane matrices, respectively, at 10 K (a); the v_4 fundamentals at 876 and 647 cm^{-1} as well as the $v_4 + \alpha$ combination bands (918 cm^{-1}) are also shown.

Fig. 3. New absorption features of the silylsilylenyl radical (HSiSiH$_2$, X^{2}A) isomer at 651 cm^{-1} (a) and of the d3-silylsilylenyl radical (DSiSiD$_2$, X^{2}A) isomer (b) at 493 cm^{-1} in the silane and d4-silane matrice at 10 K. The absorptions at 528 and 540 cm^{-1} can be attributed to the D$_3$SiSiD and SiD$_3$ species.

estimation by Sari's et al., which suggested that the bridged H$_2$SiHSi(X^{2}A″) isomer is the energetically most stable ones followed by H$_2$SiSiH(X^{2}A) (+1 kJ mol^{-1}) and H$_3$SiSi(X^{2}A″) (+13 kJ mol^{-1}), our investigation suggests that all three isomers range within 0.5 kJ mol^{-1}. Note that we have used aug-cc-pVTZ basis set which involves diffuse functions and is larger than the ones by Sari's et al. Although they have estimated the relative energies by using coupled cluster method including full triple excitations, our values with CCSD(T) method would be reasonably accurate within the accuracy of ±5 kJ mol^{-1}. The molecular structures are almost identical with Sari's paper. The vibrational frequencies obtained by Sari et al. are overestimated due to the smaller basis set than ours.

After the irradiation, the sample was kept at 10 K for one hour and was warmed up then with 0.5 K min^{-1} to 293 K. Once the silane matrix has sublimed at about

80 K, we detected additional peaks at 898 cm^{-1} (silane experiment) and 658 cm^{-1} (d4-silane experiment). These frequencies can be compared now with the calculated ones (Tables 2 and 3); we identify the 898 and 658 cm^{-1} absorptions as the most intense v_{11} (symmetric SiH$_2$/SiD$_2$ bending) fundamental of the thermodynamically most stable H$_2$SiSiH$_2$(X^{1}A$_g$) isomer and its perdeuterated counterpart (Fig. 4).

5. Discussion and summary

Our combined experimental and theoretical investigation verify that the reaction sequence (1)–(3) to form the disilyl radical, Si$_2$H$_5$(X^{2}A′), is followed by a consecutive radiolysis of the disilyl radical to synthesize the silylsilylene isomer, H$_3$SiSiH(X^{1}A′), at 10 K (Fig. 5). This molecule and its perdeuterated isotopomers have
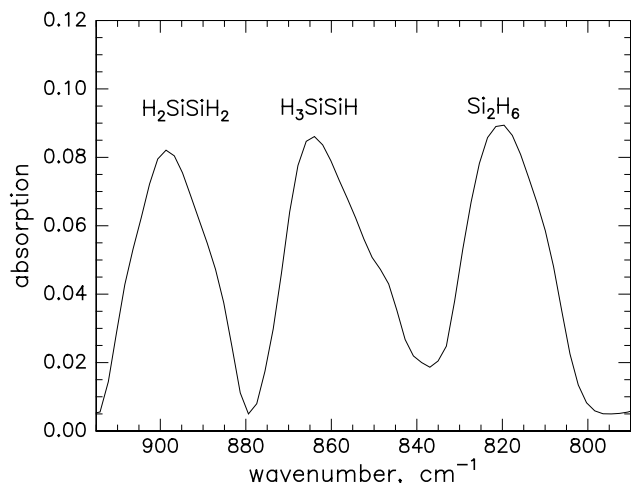
Fig. 4. Absorption features of the silylsilylene (HSiSiH$_3$, X^{1}A′) isomer at 867 cm^{-1} and of disilene (H$_2$SiSiH$_2$, X^{1}A$_g$) at 898 cm^{-1} after the sublimation of the silane matrix. The absorption of disilane at 820 cm^{-1} is also shown.

been identified though their v_5 fundamentals at 867 and 635 cm^{-1}, respectively. In the warm up phase of the system after the actual irradiation, we are also able to observe the v_{11} absorptions of the thermodynamically most stable Si$_2$H$_4$ isomer, disilene H$_2$SiSiH$_2$(X^{1}A$_g$), and its isotopomer at 898 cm^{-1} (SiH$_4$ experiment) and 658 cm^{-1} (SiD$_4$ experiment). We try to answer now the question if both isomers are produced via an atomic hydrogen loss from the disilyl radical at 10 K and the fundamentals of H$_2$SiSiH$_2$(X^{1}A$_g$) are only obscured by the absorption of the silane matrix. Or is the silylsilylene species the only isomer being formed at 10 K? Integrating the v_5 and v_{11} fundamentals and accounting for the integral absorption coefficients of these bands, we find a ratio of the H$_2$SiSiH$_2$(X^{1}A$_g$) to H$_3$SiSiH(X^{1}A′) of about one after the silane matrix has sublimed. Additionally, the number of H$_3$SiSiH(X^{1}A′) species per cm^2

sample does not decrease while the matrix is being annealed. These data suggest that both isomers are formed at 10 K; an isomerization of the H$_3$SiSiH(X^{1}A′) isomer to the H$_2$SiSiH$_2$(X^{1}A$_g$) structure can be likely ruled our since the intensity of the v_5 fundamental does not change once the sample is warmed up. This interpretation gains also support from previous matrix studies of the Si$_2$H$_4$ system [18]. Here, H$_3$SiSiH (X^{1}A′) was found to isomerize to H$_2$SiSiH$_2$(X^{1}A$_g$) only via a photon induced [1,2]-H-migration, but not thermally. The authors calculated also the thermal isomerization pathway. Actually, this process involves the bridged isomer, H$_2$SiHSiH(X^{1}A), which was clearly not observed in our experiments. Also, a barrier of 33 kJ mol^{-1} had to be overcome. This is certainly not feasible in our system: the infrared spectrum of both the H$_2$SiSiH$_2$(X^{1}A$_g$) and H$_3$SiSiH(X^{1}A′) isomers (Fig. 4) was taken at about 70 K. This temperature corresponds to 0.6 kJ mol^{-1}. Assuming a Maxwell–Boltzman distribution of the thermalized H$_3$SiSiH(X^{1}A′) isomer at $T = 70$ K, less than 1% of the H$_3$SiSiH(X^{1}A′) isomers can isomerizes thermally to H$_2$SiSiH$_2$(X^{1}A$_g$). Also, considering the differences of the enthalpies of formation of both Si$_2$H$_4$ isomers of 27 ± 5 kJ mol^{-1}, we would expect a H$_2$SiSiH$_2$(X^{1}A$_g$) to H$_3$SiSiH(X^{1}A′) ratio of about 10^{19}. This is clearly not the case. Therefore, we must conclude that in our studies, both experimentally observed Si$_2$H$_4$ isomers are formed via non-equilibrium, suprathermal processes at 10 K through a silicon–hydrogen bond rupture within the disilyl radical. We would like to stress that we averaged the infrared spectra over 180 s each. Therefore, we cannot exclude that to a minor amount H$_2$SiSiH$_2$(X^{1}A$_g$) and H$_3$SiSiH(X^{1}A′) are formed via concerted four center [1,2] and three center [1,1] molecular hydrogen elimination pathways. Future experiments employing H$_3$SiSiD$_3$ will solve this remaining question.
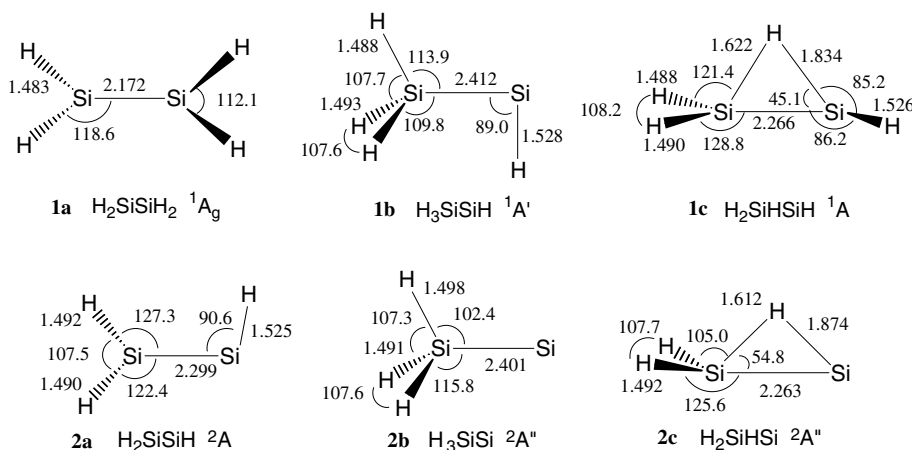
Fig. 5. Optimized structures of Si$_2$H$_4$ and Si$_2$H$_3$ species calculated with the B3LYP/6-311G(d,p) method. The bond lengths and angles are given in units of Å and °, respectively.

Upon further irradiation of the sample, the Si_2H_4 isomers were found to be radiolyzed to the Si_2H_3 radical $H_2SiSiH(X^2A)$; the latter has been assigned via the ν_5 fundamental. Neither the $H_2SiHSi(X^2A'')$ nor the $H_3SiSi(X^2A'')$ isomers could be identified since their absorptions overlap with the silane matrix and with the disilyl radical. Even upon a sublimation of the matrix, the elusive Si_2H_3 structures could not be detected. Recall that the $H_2SiSiH_2(X^1A_g)$ and $H_3SiSiH(X^1A')$ precursors were formed in a 1:1 ratio. A simply Si–H bond rupture in $H_2SiSiH_2(X^1A_g)$ would lead solely to the experimentally observed $H_2SiSiH(X^2A)$ isomer. The $H_3SiSiH(X^1A')$ structure has two non-equivalent silicon–hydrogen bonds. If the Si–H bond is cleaved statistically, we expect a $H_2SiSiH(X^2A)$ to $H_3SiSi(X^2A'')$ ratio of 3:1. These thoughts postulate a dominant formation of $H_2SiSiH(X^2A)$ as verified experimentally. The present study completes the gap in the infrared spectroscopic characterization of small hydrogenated silicon clusters Si_2H_y ($y = 3–6$). The new infrared absorption of the $H_2SiSiH(X^2A)$ radical may be employed in future spectroscopic investigations of chemical vapor deposition processes and in astronomical searches in the infrared regime toward the carbon star IRC + 10216.

Acknowledgements

References

[1] R. Prasad, N. Chakraborti, Met. Mater. Proc. 10 (1998) 203.
[2] P. Ho, M.E. Coltrin, J.S. Binkley, C.F. Melius, J. Phys. Chem. 90 (1986) 3399.
[3] M.C. Ernst, A.F. Sax, J. Kalcher, Chem. Phys. Lett. 216 (1993) 189.
[4] M.T. Swihart, J. Phys. Chem. A 104 (2000) 6083.
[5] X.G. Gong, D. Guenzeburger, E.B. Saitovitch, Chem. Phys. Lett. 275 (1997) 392.
[6] C. Pak, J.C. Rienstra-Kiracofe, H.F. Schaefer, J. Phys. Chem. A 104 (2000) 11232.
[7] G.R. Gupte, R. Prasad, Int. J. Mod. Phys. B 12 (1998) 1607.
[8] T. Shirafuji et al., Jpn. J. Appl. Phys. 32 (1993) 1546.
[9] J.G.E. Gardeniers, L.J. Giling, F. De Jong, J.P. van der Eerden, J. Cryst. Growth 104 (1990) 727.
[10] S.L. Girshickm, M.T. Swihart, S.M. Shu, M.R. Mahajan, S. Nijhawan, Proc. Electrochem. Soc. 98 (1999) 215.
[11] M.T. Swihart, S.L. Girshick, J. Phys. Chem. B 103 (1999) 64.
[12] A. Matsuda, K. Tanaka, Thin Solid Film 92 (1982) 172.
[13] Z.X. Wang, M.B. Haung, J. Chem. Soc., Faraday Trans. 94 (1998) 635.
[14] S. Oikawa, M. Tsuda, S. Ohtsuka, J. Mol. Struct. 310 (1994) 287.
[15] B. Ruscic, J. Berkowitz, J. Chem. Phys. 95 (1991) 2416.
[16] L. Andrews, X. Wang, J. Phys. Chem. A 106 (2002) 7696.
[17] D. Sillars, C. Bennett, R.I. Kaiser, Y. Osamura, Chem. Phys. 2004 (in press).
[18] G. Maier, H.P. Reisenauer, J. Glatthaar, Chem. Eur. J. 8 (2002) 4383.
[19] L. Sari, M.C. McCarthy, H.F. Schaefer, P. Thaddeus, J. Am. Chem. Soc. 125 (2003) 11409.
[20] B.E. Turner, Astrophys. J. 376 (1991) 573.
[21] R.I. Kaiser, Chem. Rev. 102 (2002) 1309.
[22] D.M. Goldhaber, A.L. Betz, Astrophys. J. 279 (1984) L55.
[23] C. Bennett, A.M. Mebel, R.I. Kaiser, Phys. Chem. Chem. Phys., 2004 (submitted).
[24] W.M. Sears, J.A. Morrison, J. Chem. Phys. 62 (1975) 2736.
[25] A.D. Becke, J. Chem. Phys. 98 (1993) 5648.
[26] C. Lee, W. Yang, R.G. Parr, Phys. Rev. B 37 (1988) 785.
[27] R. Krishnan, J.S. Binkley, R. Seeger, J.A. Pople, J. Chem. Phys. 72 (1980) 650.
[28] N. Chakraborti, P.S. de, R. Prasad, Z. Metallkunde 90 (1999) 7.
[29] J. Cizek, Adv. Chem. Phys. 14 (1969) 35.
[30] J.A. Pople, M. Head-Gordon, K. Raghavachari, J. Chem. Phys. 87 (1987) 5968.
[31] R.A. Kendall, T.H. Dunning, R.J. Harrison, J. Chem. Phys. 96 (1992) 6796.
[32] M.J. Frisch et al., GAUSSIAN 98 Revision A11, Gaussian, Pittsburgh, PA, 2002.
[33] L. Andrews, X. Wang, J. Phys. Chem. A 106 (2002) 7696.
[34] L. Li, J.T. Graham, W. Weltner, J. Phys. Chem. A 105 (2001) 11018.
[35] N. Legay-Sommaire, F. Legay, J. Phys. Chem. A 102 (1998) 8759.